

Mechanism Shift During Post-training from Autoregressive to Masked Diffusion Language Models

Injin Kong^{1,*} Hyoungjoon Lee^{2,*} Yohan Jo^{1,†}

¹Graduate School of Data Science, Seoul National University

²Department of Biosystems & Biomaterials Science and Engineering, Seoul National University
mtkong77@snu.ac.kr, hjoon721@snu.ac.kr, yohan.jo@snu.ac.kr

Abstract

Post-training pretrained Autoregressive models (ARMs) into Masked Diffusion models (MDMs) has emerged as a cost-effective strategy to overcome the limitations of sequential generation. However, the internal algorithmic transformations induced by this paradigm shift remain unexplored, leaving it unclear whether post-trained MDMs acquire genuine bidirectional reasoning capabilities or merely repack-age autoregressive heuristics. In this work, we address this question by conducting a comparative circuit analysis of ARMs and their MDM counterparts. Our analysis reveals a systematic “mechanism shift” dependent on the **structural nature of the task**. Structurally, we observe a distinct divergence: while MDMs largely retain autoregressive circuitry for tasks dominated by local causal dependencies, they abandon initialized pathways for global planning tasks, exhibiting distinct rewiring characterized by increased early-layer processing. Semantically, we identify a transition from **sharp**, localized specialization in ARMs to **distributed** integration in MDMs. Through these findings, we conclude that diffusion post-training does not merely adapt model parameters but fundamentally reorganizes internal computation to support **non-sequential global planning**.

1 Introduction

Large language models have achieved near-human performance across diverse linguistic tasks (OpenAI et al., 2024; Qwen et al., 2025; Touvron et al., 2023). Despite these advances, the prevalent autoregressive framework (Vaswani et al., 2017; Radford et al., 2019) imposes structural limitations on generation (Welleck et al., 2019; Bengio et al., 2015). Specifically, sequential generation under causal masking prevents correcting past tokens (Gu et al., 2018; Welleck et al., 2019; Vaswani et al.,

2017) so that early errors propagate and amplify throughout the sequence, as the model cannot correct past inaccuracies (Bengio et al., 2015; Ranzato et al., 2016). Moreover, many reasoning and planning tasks require global reasoning, where early decisions must account for constraints that apply to the entire sequence (Gu et al., 2018; Ye et al., 2025a).

Masked diffusion models (MDMs) have gained increasing interest as a non-autoregressive paradigm, with structural properties well-suited to overcoming these limitations (Austin et al., 2021; Sahoo et al., 2024). However, training diffusion-based language models from scratch remains computationally expensive due to slower convergence (Gong et al., 2025). To mitigate this cost, recent work proposes post-training pretrained autoregressive models (ARMs) to the diffusion paradigm (Gong et al., 2025; Ye et al., 2025b). Models such as Dream (Ye et al., 2025b) demonstrate that this strategy can achieve strong performance while requiring only a fraction of the compute needed for training from scratch.

Despite the empirical success of post-training ARMs with diffusion objectives, the specific algorithm changes induced by this post-training process are not yet understood (Gong et al., 2025). It remains unclear whether post-trained MDMs genuinely learn new bidirectional reasoning mechanisms, as intended by the diffusion framework, or instead still rely heavily on autoregressive mechanisms at their core. Although mechanistic interpretability has been applied to understand diffusion models for image generation (Shi et al., 2025; Niedoba et al., 2025), this level of analysis has not yet been extended to text diffusion. Without such analysis, it is difficult to determine if post-trained MDMs genuinely perform global reasoning. If models continue to rely on local, left-to-right heuristics, the theoretical benefits of diffusion-based architectures fail to materialize.

*Equal contribution.

†Corresponding author.

In this work, we address this question by analyzing language models from a circuit-level perspective (Bhaskar et al., 2024), which allows us to directly examine whether diffusion post-training induces new computational pathways or primarily reuses existing autoregressive ones. We investigate **where** algorithmic changes occur by comparing circuit structures between ARMs and MDMs post-trained from the same autoregressive backbones, and then examine **how** these changes are realized through detailed analysis using logit lens techniques and neuron-level visualizations.

Through this analysis, we demonstrate that post-training using MDM objectives does not merely alter the training loss but instead induces a systematic reorganization of internal computation—shifting semantic roles across components and revealing a mechanism shift in how language models process and refine linguistic information.

2 Related Works

2.1 Masked Diffusion Models

MDMs generate text by reversing a corruption process that stochastically replaces tokens with a [MASK] symbol (Chang et al., 2022; Austin et al., 2021). This approach allows for non-autoregressive generation using full bidirectional context.

While training such models from scratch (Nie et al., 2025) is computationally expensive, recent work has shown that pretrained ARMs can be effectively post-trained into MDMs (Gong et al., 2025). Rather than learning diffusion dynamics from scratch, these approaches initialize from a pretrained ARM. The model is then post-trained to iteratively denoise partially masked inputs, instead of predicting the next token autoregressively. From DiffuLLaMA (Gong et al., 2025) to Dream (Ye et al., 2025b), this line of work shows that post-training pretrained ARMs to MDM objectives can retain many practical advantages of diffusion—such as parallel decoding, iterative refinement, and bidirectional attention—while substantially reducing training cost. Post-trained MDMs also achieve strong performance on directionality-sensitive tasks. However, while these works establish the effectiveness of post-trained MDMs, they largely focus on performance and efficiency, leaving open the question of how diffusion objectives reshape the underlying computational mechanisms.

2.2 Mechanistic Interpretability and Circuits

Mechanistic interpretability aims to identify the internal components and algorithms responsible for specific model behaviors (Olah et al., 2020; Elhage et al., 2021). A central concept is the **circuit**, defined as a subgraph of the computational graph connecting inputs to the unembedding projection that is sufficient to produce a target behavior (Olah et al., 2020; Bhaskar et al., 2024). Nodes correspond to components such as attention heads and MLPs, while directed edges represent causal dependencies between components, where the output of one node contributes to the input of another (Ou et al., 2025; Hanna et al., 2024).

Empirical studies show that many behaviors can be explained by sparse circuits involving only a small fraction of model connections (Bhaskar et al., 2024; Wang et al., 2023). Methods such as Edge Attribution Patching identify these subgraphs via gradient-based attribution, enabling circuit discovery for tasks including indirect object identification and numerical comparison (Hanna et al., 2023; Lieberum et al., 2023; Bhaskar et al., 2024). Across models and scales, similar circuits—such as induction heads—recur consistently, suggesting that they implement stable algorithmic functions rather than incidental patterns (Prakash et al., 2024; Tigges et al., 2024; Ou et al., 2025; Wang et al., 2025). Recent automated approaches, including ACDC and EAP, further enable scalable circuit discovery without manual inspection (Syed et al., 2024; Bhaskar et al., 2024).

While mechanistic analyses have begun to probe diffusion models in the vision domain (Shi et al., 2025; Niedoba et al., 2025), comparable studies for text diffusion models remain limited. As a result, it is unclear whether diffusion objectives induce distinct computational strategies in language models or primarily reorganize existing autoregressive circuitry.

3 Method

To investigate the mechanistic shift from ARMs to MDMs, we adopt a comparative framework. Our primary objective is to distinguish the impact of shifting the learning objective from causal modeling to masked diffusion on circuit topology. We control for architectural confounding by analyzing ARMs alongside their directly post-trained MDM counterparts.

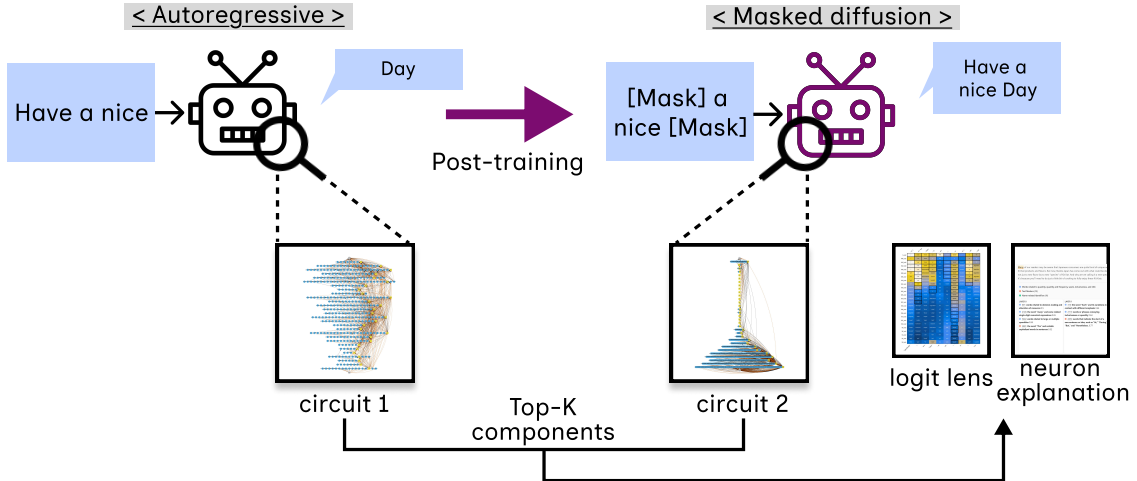


Figure 1: **Overview of the mechanism shift analysis pipeline.** We extract task-specific circuits for both the **Autoregressive Model (ARM)** baseline and the post-trained **Masked Diffusion Model (MDM)**. We then identify the **Top-K components** that exhibit the highest topological divergence between the two architectures. Finally, we interpret the algorithmic nature of these shifts using **Logit Lens** and **Neuron Explanation**.

3.1 Models and Configuration

We conduct experiments across two distinct model families to verify the generalizability of our findings. Specifically, we utilize the **Qwen2.5-7B** (Qwen et al., 2025) and **LLaMA-2-7B** (Touvron et al., 2023) architectures.

To enable a direct comparison, we pair each standard autoregressive checkpoint with an MDM post-trained from that specific ARM base:

- **Qwen Series:** We compare the autoregressive Qwen2.5-7B against Dream-Base-7B (Ye et al., 2025b), an MDM post-trained from the Qwen backbone.
- **LLaMA Series:** We compare the autoregressive LLaMA-2-7B against DiffuLLaMA-7B (Gong et al., 2025), which was initialized from LLaMA 2 weights.

3.2 Tasks and Datasets

We analyze circuit behavior on two distinct tasks to highlight different performance capabilities: one focused on autoregressive causal dependencies and another on global reasoning. Additional details for tasks and datasets are provided in Appendix A.

Indirect Object Identification (IOI): A canonical interpretability task primarily solved by **Induction Heads** in ARMs (Wang et al., 2023). We select this task to serve as a representative baseline for **causal reasoning**; specifically, we aim to in-

vestigate whether the induction circuitry—which inherently relies on sequential, left-to-right context to copy tokens—persists, dissolves, or transforms when the training objective shifts from causal prediction to masked diffusion.

Countdown: A numerical reasoning task where the model is provided with a set of integers and a target value and must generate a valid arithmetic equation using the inputs to equal the target (Ye et al., 2025a). This task serves as a critical benchmark for **global reasoning** because it requires inverse planning—decisions made early in the sequence must be strictly conditioned on the final goal—thereby challenging the left-to-right causality of ARMs while favoring the bidirectional context and global refinement capabilities of MDMs.

Inference Configuration For all experiments, we use task-dependent generation lengths. For IOI, we use a single diffusion step, while for COUNT-DOWN, we align diffusion steps with the target sequence length. Details are provided in Appendix A.

3.3 Circuit Discovery and Analysis Pipeline

We hypothesize that the transition to masked diffusion induces specific algorithmic shifts in tasks where MDMs outperform ARMs (e.g., Countdown). To verify this, we employ a three-stage pipeline: Discovery, Topological Comparison, and Mechanism Interpretation. This workflow allows us to first locate where the computation changes

and then analyze what those changes represent semantically.

3.3.1 Discovery

We employ automated circuit discovery based on Edge Attribution Patching with Integrated Gradients (EAP-IG) (Hanna et al., 2024) to identify the minimal computational subgraph responsible for task performance. For a given task, we identify a sparse subgraph $\mathcal{C} \subset \mathcal{G}$ containing the subset of edges required to keep the model’s performance within a threshold τ of the full model. Within this discovered circuit, **nodes** represent distinct functional components: attention heads primarily act as information movers that copy content from preceding tokens, while MLPs often serve as associative memories that extract or refine specific semantic attributes from the input state. Consequently, the **edges** structurally define the algorithmic logic, specifying how these functional outputs are composed and routed to produce the final prediction.

3.3.2 Attribution-Guided Circuit Comparison

To localize *where* algorithmic changes concentrate when transitioning from ARMs to MDMs, we leverage EAP-IG to compare circuits at the level of edges and their incident components. Rather than treating all discovered edges equally, we focus on those that carry the highest attribution mass under EAP-IG and then identify which components are repeatedly used as sources or sinks of these high-attribution edges.

EAP-IG Edge Overlap: For each model (ARM and MDM), we first select the set of top-attribution edges (1000 edges), $\mathcal{E}_{\text{ARM}}^{\text{top}}$ and $\mathcal{E}_{\text{MDM}}^{\text{top}}$, by ranking edges according to their EAP-IG scores on identical prompts. We then quantify overlap using the Jaccard similarity $J(\mathcal{E}_{\text{ARM}}^{\text{top}}, \mathcal{E}_{\text{MDM}}^{\text{top}}) = |\mathcal{E}_{\text{ARM}}^{\text{top}} \cap \mathcal{E}_{\text{MDM}}^{\text{top}}| / |\mathcal{E}_{\text{ARM}}^{\text{top}} \cup \mathcal{E}_{\text{MDM}}^{\text{top}}|$. High overlap suggests that the MDM reuses the same high-attribution pathways as the ARM, whereas low overlap indicates that diffusion training recruits a distinct set of edges to implement its generative computation. The choice of selecting the top 1000 edges reflects a trade-off between attribution coverage and circuit sparsity and is empirically justified in Appendix B.

Top-K EAP-IG Components: To move from edges to components, we assign each node v a score $s(v)$ by aggregating the EAP-IG scores of all incident edges, defined as the sum of incoming attributions $\sum_{(u,v) \in \mathcal{E}^{\text{top}}} \text{EAP-IG}(u \rightarrow v)$ and

outgoing attributions $\sum_{(v,u) \in \mathcal{E}^{\text{top}}} \text{EAP-IG}(v \rightarrow u)$, where \mathcal{E}^{top} denotes the set of top-attribution edges for the model. In words, a component is important if it repeatedly appears as either the source or the target of high-scoring EAP-IG edges. We then define the **Top-K Components** (with $K = 100$) for each model as the nodes with the largest $s(v)$. The choice of K is empirically motivated and discussed in Appendix B.

Based on these metrics, we first assess the degree of circuit reuse between ARMs and MDMs via overlap of high-attribution edges. High edge overlap provides evidence of mechanistic recycling, where the MDM relies on pre-trained autoregressive pathways, while low overlap indicates the emergence of diffusion-specific generative strategies. Within these regions, the Top-K EAP-IG Components pinpoint nodes that sit at the endpoints of the most influential edges, yielding a focused set of components for downstream mechanistic analysis via logit lens and neuron-level visualization.

3.3.3 Mechanism Interpretation

Having identified *where* the circuit changes, we investigate *how* the computation differs by applying interpretability techniques specifically to the Top-K Divergent Components:

Logit Lens and Component-wise Analysis: Following the logit lens framework (nostalgebraist, 2020), we project intermediate activations into the vocabulary space via the unembedding matrix W_U , yielding $P_{\text{AR}}(x | c, t) = \text{softmax}(W_U h_{\text{component}}^{(c,t)})$ and $P_{\text{MDM}}(x | c, t, s) = \text{softmax}(W_U h_{\text{component}}^{(c,t,s)})$, where c indexes a component (e.g., an attention head), t denotes the token position, and s the diffusion timestep.

For autoregressive models (Qwen, LLaMA), we apply the component-wise logit lens to all token positions in the sequence on both IOI and COUNT-DOWN tasks. This enables us to trace how the model’s internal representation becomes aligned with the target output across the sequence and to decompose the contributions of the residual stream, attention heads, and MLPs at each token position.

For MDMs (Dream, DiffuLLaMA), we examine how these component-wise projections evolve across the diffusion time steps at a fixed set of token positions. Dream supports per-head and per-MLP decompositions, while DiffuLLaMA is analyzed at the level of residual, attention, MLP, and residual-out layers.

This analysis allows us to assess whether a given component has shifted its semantic role—for example, from contributing primarily to next-token prediction in an ARM to encoding a global target or distant operator in an MDM—and how such semantic alignment emerges progressively over diffusion time. Importantly, when applying the unembedding matrix to intermediate component activations, we do not interpret the resulting logits as the model’s final predictions. Instead, they serve as a diagnostic probe that reveals which tokens a component is linearly aligned with at a particular stage of computation.

Neuron Explanation: In this work, we define a “neuron” as a single scalar coordinate in the model’s residual stream at a given transformer layer (i.e., one element of the hidden dimension of the layer output). For both the IOI and COUNTDOWN settings, we record activations for all combinations of layers, neuron indices, and token positions on the evaluation data. Following the methodology of Bills et al. (2023), we then extract the input tokens that elicit the largest-magnitude activations for a given neuron and use these highly activating examples for qualitative inspection and automated explanation.

We focus this fine-grained analysis on the Top-K Divergent Components identified in the previous step: specifically, for divergent MLP layers, we visualize the top activating neurons to understand the specific attributes they extract; for divergent Attention layers, we analyze the head’s output features to determine what information is being moved. The primary goal of this visualization is to characterize the semantic feature selectivity of the circuit. By mapping high-activation neurons to their corresponding tokens, we aim to determine if MDM components have learned to encode non-causal features (e.g., attending to or encoding “future target” tokens available during the diffusion process) that are fundamentally inaccessible to the standard autoregressive model.

4 Results & Analysis

4.1 Circuit-Level Differences

Figure 2 illustrates the circuit structures extracted for both ARMs and MDMs across the IOI and COUNTDOWN tasks, where each circuit represents the average structure aggregated over multiple prompts and diffusion steps.

Table 1: Circuit similarity between ARMs and their post-trained MDM counterparts. Higher values indicate greater reuse of autoregressive circuitry.

Setting	Edge Overlap	Top- K Overlap
IOI (Qwen / Dream)	0.193	0.105
IOI (LLaMA-2 / DiffuLLaMA)	0.088	0.124
COUNTDOWN (Qwen / Dream)	0.008	0.093
COUNTDOWN (LLaMA-2 / DiffuLLaMA)	0.032	0.081

For the IOI task, the overall circuit topology of Dream closely resembles that of Qwen, with dominant interactions concentrated in similar layers and mediated by comparable attention pathways. A similar pattern is observed for DiffuLLaMA relative to its LLaMA-2 counterpart. This indicates that, for tasks primarily driven by local or causal dependencies—such as IOI, which effectively requires only shallow or single-step generation—post-trained MDMs largely preserve the autoregressive circuitry inherited from their ARM initializations.

This qualitative similarity is further supported by quantitative circuit similarity metrics reported in Table 1. Across both model families, the IOI task exhibits consistently higher overlap in high-attribution edges and Top- K components compared to the COUNTDOWN task, indicating substantial mechanistic reuse rather than the emergence of new diffusion-specific circuitry in tasks dominated by local dependency structures.

In contrast, the COUNTDOWN task exhibits a clear shift in circuit organization between ARMs and MDMs. In the COUNTDOWN task, the ARM circuit becomes increasingly dense toward mid-to-late layers, whereas the MDM circuit concentrates a larger fraction of interactions in early layers, resulting in a front-loaded organization of computation. This redistribution is consistently observed both in the aggregated circuit statistics (Figure 2) and in the representative circuit visualizations (Figure 3), indicating a systematic reallocation of computation under the diffusion objective.

This depth-wise shift toward increased early-layer engagement is consistently observed across both model families, with Dream and DiffuLLaMA exhibiting increased early-layer engagement compared to their respective autoregressive baselines. Quantitatively, this divergence

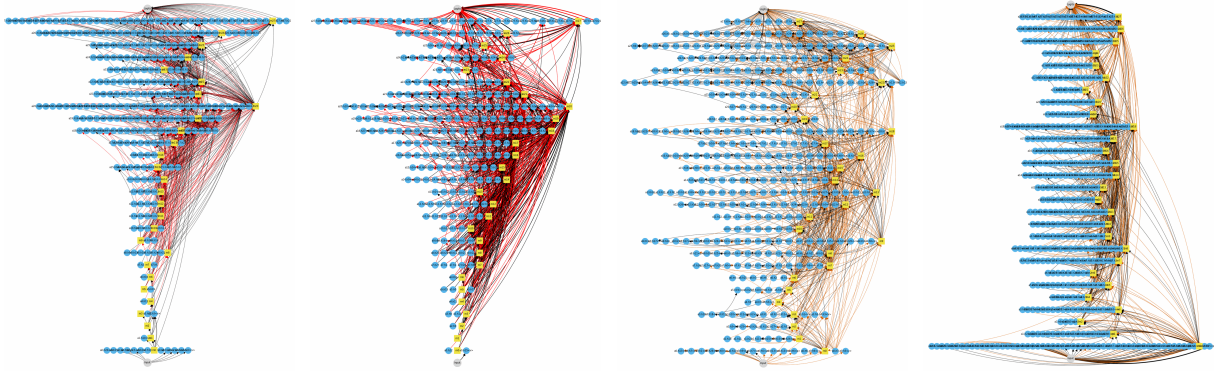


Figure 2: Circuit comparison across tasks and architectures. From left to right: IOI (Qwen2.5-7B), IOI (Dream-Base-7B), COUNTDOWN (Qwen2.5-7B), and COUNTDOWN (Dream-Base-7B).

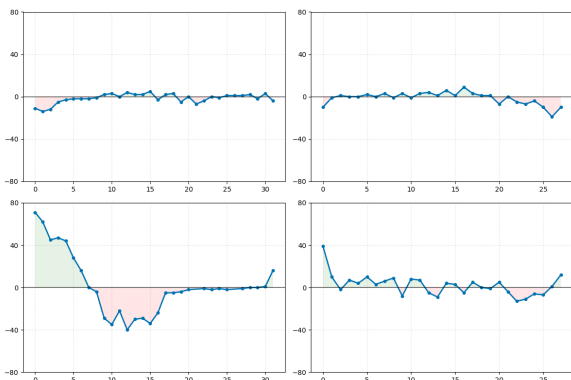


Figure 3: Layer-wise difference in unique attention component usage (MDM minus ARM). **Rows:** IOI (top) vs. COUNTDOWN (bottom). **Columns:** DiffuLLaMA vs. LLaMA-2 (left) and Dream vs. Qwen (right). **Green** regions (> 0) indicate that the diffusion model utilizes more attention heads, while **red** regions (< 0) indicate greater usage by the autoregressive model.

is reflected in markedly lower edge-level and component-level overlap scores for the COUNTDOWN task (Table 1), indicating that diffusion post-training induces non-trivial reorganization of the underlying circuitry.

Together, these results reveal a clear dichotomy in how masked diffusion post-training reshapes internal circuitry. For tasks dominated by local, causal dependencies such as IOI, post-trained MDMs retain a substantial fraction of the original autoregressive circuitry. High overlap in both edge-level attribution and Top- K components indicates that the causal reasoning machinery learned during autoregressive pre-training remains functionally effective and is therefore reused rather than replaced.

In contrast, for tasks requiring global constraint satisfaction, such as COUNTDOWN, the autoregressive circuitry proves insufficient. Here, dif-

fusion post-training induces the emergence of distinct early-layer components that are largely absent from the original ARM circuits, accompanied by a marked collapse in circuit overlap. These newly emphasized early-layer components become the primary substrates for computation, suggesting that MDMs restructure their internal mechanisms to support global planning by front-loading computation rather than relying on sequential, causal pathways.

Taken together, these findings demonstrate that masked diffusion post-training does not simply overwrite autoregressive mechanisms. Instead, it selectively preserves causal circuitry where it remains compatible with the task, while inducing genuinely new, diffusion-specific components when global reasoning demands exceed the expressive capacity of autoregressive computation.

4.2 Semantic Reorganization of Task-Critical Components and Early Layers

To understand how circuit-level differences translate into concrete computational strategies, we analyze model behavior at two complementary granularities. First, we examine **task-critical components**—attention heads and MLPs that receive high EAP-IG attribution—using component-wise logit lens analysis. This allows us to characterize how semantic roles are assigned to components that directly influence task outputs. Second, we analyze **early-layer neuron activations** to understand how these semantic roles are implemented internally, particularly in regions where MDMs emphasize computation but component-level semantics appear diffuse.

Table 2: Representative components exhibiting high logit concentration across tasks and model families. Roles are descriptive labels summarizing observed logit distribution patterns rather than definitive functional assignments.

Task	Model	Component	Mean Logit	Top Tokens	Role
IOI	Qwen	a27.h5	21.14	Dan	Person-name-related Component
	Qwen	a23.h11	6.84	Ben	Person-name-related Component
	LLaMA	a24.h15	2.75	Jerry	Person-name-related Component
	LLaMA	a21.h1	1.73	Carol	Person-name-related Component
	Dream	m25	3.14	Browser	Proper-noun component
	Dream	m22	2.33	Kremlin	Proper-noun component
	DiffuLLaMA	a26.h21	2.81	Marian	Person-name-related Component
	DiffuLLaMA	a22.h19	1.80	Grace	Person-name-related Component
COUNTDOWN	Qwen	m25	51.29	3	Digit-related Component
	Qwen	m20	20.67	1, 2	Broad Numerical Component
	LLaMA	m29	6.20	pick	Instruction-related Component
	LLaMA	a22.h13	2.10	four	Numerical–Lexical Component
	Dream	m27	26.06	1, 2, 3	Broad Numerical Component
	Dream	m23	5.34	5, 1, 4	Broad Numerical Component
	DiffuLLaMA	m31	12.32	0, 1, 2	Broad Numerical Component
	DiffuLLaMA	m4	1.40	–	Symbol-related Component

4.2.1 Task-Critical Components: Component-wise Logit Lens Analysis

We begin by analyzing components that directly contribute to task performance, as identified by high EAP-IG attribution. By applying a component-wise logit lens to these components, we probe their semantic alignment with output tokens, allowing us to assess whether task-relevant information is concentrated within a small number of specialized components or distributed across many.

Causal reasoning task (IOI) For the IOI task, ARMs exhibit **sharply localized semantic specialization**. In both Qwen and LLaMA, a small number of attention heads are strongly aligned with person-name tokens (e.g., *Dan*, *Jerry*), producing large-magnitude logits that dominate prediction. This pattern indicates that IOI is largely solved by a limited set of highly specialized components that act as deterministic, pointer-like mechanisms.

DiffuLLaMA largely preserves this behavior. Several high-attribution components remain strongly aligned with person-name tokens and exhibit logit profiles comparable to those of the underlying ARM. This suggests substantial inheritance of autoregressive circuitry, consistent with the observation that IOI relies primarily on local causal dependencies that are already well supported by the autoregressive objective.

Dream, however, departs from this pattern. Its high-attribution components do not exhibit clear person-name specificity. Instead, the strongest logit alignments correspond to non-person proper

nouns or broader semantic tokens (e.g., *Browser*, *Kremlin*). This indicates that, despite similar circuit topology at a coarse level, diffusion post-training redistributes semantic roles across components, weakening the dominance of individual name-specific heads.

Global reasoning task (Countdown). A contrasting pattern emerges in the COUNTDOWN task. ARMs rely on components with **strong numerical selectivity**, often sharply aligned with specific digits or operators. These components produce high-confidence logits concentrated on a narrow subset of tokens, indicating that global planning is approximated through sequential, component-centric heuristics.

In Dream, this sharp specialization collapses. Instead of a single dominant numerical component, multiple components exhibit moderate logit responses distributed across numerical tokens, with no individual component exerting decisive control over prediction. DiffuLLaMA again occupies an intermediate regime, retaining numerical associations but with reduced magnitude and increased dispersion.

Taken together, these results indicate that diffusion post-training induces a **semantic reorganization at the component level**. Whereas ARMs resolve tasks through a small number of highly specialized components, MDMs—particularly on global reasoning tasks—redistribute semantic responsibility across multiple components, yielding a more ensemble-like computation.

4.2.2 Early-layer Representation: Neuron-level Analysis

While component-wise logit lens analysis captures semantic specialization among task-critical components, it does not fully explain the behavior of early-layer regions that are emphasized by masked diffusion circuits. To characterize how task-relevant information is implemented in these layers, we analyze neuron activations in the lowest transformer layers across tasks and model classes.

In ARMs, neuron activation in early layers is **highly task-dependent**. In the IOI task, a large number of neurons in early layers are strongly activated by descriptive adjectives and modifier-related tokens, suggesting that early layers encode fine-grained syntactic and descriptive features prior to resolving entity identity. In the COUNTDOWN task, this pattern shifts markedly toward neurons associated with numerical or technical content. Despite this task-dependent reallocation, ARMs consistently exhibit strong concentration within specific semantic categories.

MDMs display a qualitatively different pattern. Across both IOI and COUNTDOWN, the total number of active neurons in early layers remains relatively stable. Moreover, the activated neurons tend to correspond to broad, genre-level cues—such as general numerical or technical content—rather than sharply defined task-specific categories. This indicates that MDMs rely less on early-layer specialization and instead maintain a more uniform, task-agnostic representational regime.

This contrast persists in the early layer. Across depth, ARMs repeatedly exhibit sharper category-level specialization, while MDMs maintain flatter activation profiles with fewer neurons strongly associated with any single semantic category.

4.2.3 Connecting Component-level and Neuron-level Perspectives

Component-wise logit lens and neuron-level visualization serve complementary interpretability roles. Logit lens probes **semantic alignment at the level of components**, revealing which tokens individual attention heads or MLPs are linearly aligned with and how they directly influence model outputs. Neuron-level analysis, by contrast, characterizes **how semantic information is internally implemented**, independent of direct alignment with the output vocabulary.

Together, these analyses reveal a consistent mechanistic pattern that is further supported by

quantitative differences in explanation structure. ARMs exhibit a smaller number of unique explanatory components (266) but substantially higher variance in explanations (136,738.5), indicating that model behavior is dominated by a limited set of highly influential and specialized components. In contrast, MDMs rely on a larger pool of explanatory components (426) with markedly lower variance (41,015.5), suggesting that explanatory responsibility is distributed more evenly across components.

This quantitative shift aligns with the qualitative patterns observed in both analyses. ARMs employ a component-centric strategy in which task resolution is dominated by a small number of sharply specialized attention heads, or MLPs, supported by task-specific early-layer neurons. MDMs, by contrast, replace these sharp semantic roles with distributed responsibility, activating broader sets of components whose individual contributions are weaker but collectively stable. At the neuron level, this manifests as early-layer representations that exhibit reduced task-specific selectivity and more uniform activation profiles across tasks.

Taken together, these findings provide a coherent mechanistic account of diffusion post-training. MDMs trade component-level specialization for distributed semantic coverage, supported by early layers that provide broad, task-invariant representational scaffolding. This reorganization explains both the front-loaded computation observed in circuit analyses and the absence of dominant, easily interpretable components in logit-lens probes, highlighting a fundamental shift from localized causal pathways to globally integrated computation.

5 Conclusion

In this paper, we investigated how post-training an autoregressive language model (ARM) with a masked diffusion objective reshapes its internal computational mechanisms. By combining circuit analysis, component-wise logit-lens probing, and neuron-level explanation, we provided a mechanistic comparison between ARMs and their post-trained masked diffusion model (MDM) counterparts across tasks with distinct structural demands.

Limitations

Our analysis focuses on a limited set of tasks—IOI and COUNTDOWN—which are chosen to isolate causal dependency and global planning behaviors,

respectively. While these tasks are well-established benchmarks in mechanistic interpretability, the circuits identified in this work should be interpreted as task-specific mechanisms rather than universal properties of autoregressive or masked diffusion language models. Different linguistic or reasoning tasks may recruit alternative circuitry or induce distinct patterns of post-training adaptation. In addition, our circuit discovery pipeline relies on sparsity-inducing methods such as EAP-IG and Top-K divergence selection to isolate the most behaviorally salient components. Although this design choice improves interpretability by filtering out noisy or redundant pathways, it implies that not all attention heads and MLP components are exhaustively analyzed, and secondary or auxiliary mechanisms that contribute weakly to task performance may be omitted. Finally, our approach involves an inherent trade-off between interpretability resolution and computational scalability: component-wise logit lens analysis and neuron-level visualization across diffusion steps are computationally expensive, particularly for large-scale models. As a result, we prioritize in-depth analysis of selected components over exhaustive full-model sweeps, and extending the analysis to broader component sets or additional configurations would require substantially greater computational resources.

References

- Jacob Austin, Daniel D. Johnson, Jonathan Ho, Daniel Tarlow, and Rianne van den Berg. 2021. [Structured denoising diffusion models in discrete state-spaces](#). In *Advances in Neural Information Processing Systems*.
- Samy Bengio, Oriol Vinyals, Navdeep Jaitly, and Noam Shazeer. 2015. [Scheduled sampling for sequence prediction with recurrent neural networks](#). In *Advances in Neural Information Processing Systems*, volume 28. Curran Associates, Inc.
- Adithya Bhaskar, Alexander Wettig, Dan Friedman, and Danqi Chen. 2024. [Finding transformer circuits with edge pruning](#). In *The Thirty-eighth Annual Conference on Neural Information Processing Systems*.
- Steven Bills, Nick Cammarata, Dan Mossing, Henk Tillman, Leo Gao, Gabriel Goh, Ilya Sutskever, Jan Leike, Jeff Wu, and William Saunders. 2023. Language models can explain neurons in language models. <https://openaipublic.blob.core.windows.net/neuron-explainer/paper/index.html>.
- Huiwen Chang, Han Zhang, Lu Jiang, Ce Liu, and William T. Freeman. 2022. Maskgit: Masked generative image transformer. In *The IEEE Conference on Computer Vision and Pattern Recognition (CVPR)*.
- Nelson Elhage, Neel Nanda, Catherine Olsson, Tom Henighan, Nicholas Joseph, Ben Mann, Amanda Askell, Yuntao Bai, Anna Chen, Tom Conerly, Nova DasSarma, Dawn Drain, Scott Elshohk, Tristan Hume, Sam McCandlish, Pamela Mishkin, Danny Nguyen, Chris Olah, Eric Sigler, Kyle Sommer, and Ilya Sutskever. 2021. A mathematical framework for transformer circuits. <https://transformer-circuits.pub/2021/framework/index.html>. Transformer Circuits.
- Shansan Gong, Shivam Agarwal, Yizhe Zhang, Jiacheng Ye, Lin Zheng, Mukai Li, Chenxin An, Peilin Zhao, Wei Bi, Jiawei Han, Hao Peng, and Lingpeng Kong. 2025. [Scaling diffusion language models via adaptation from autoregressive models](#). In *The Thirteenth International Conference on Learning Representations*.
- Jiatao Gu, James Bradbury, Caiming Xiong, Victor O.K. Li, and Richard Socher. 2018. [Non-autoregressive neural machine translation](#). In *International Conference on Learning Representations*.
- Michael Hanna, Ollie Liu, and Alexandre Variengien. 2023. [How does GPT-2 compute greater-than?: Interpreting mathematical abilities in a pre-trained language model](#). In *Thirty-seventh Conference on Neural Information Processing Systems*.
- Michael Hanna, Sandro Pezzelle, and Yonatan Belinkov. 2024. [Have faith in faithfulness: Going beyond circuit overlap when finding model mechanisms](#). In *First Conference on Language Modeling*.
- Tom Lieberum, Matthew Rahtz, J’anos Kram’ar, Geoffrey Irving, Rohin Shah, and Vladimir Mikulik. 2023. [Does circuit analysis interpretability scale? evidence from multiple choice capabilities in chinchilla](#). *ArXiv*, abs/2307.09458.
- Shen Nie, Fengqi Zhu, Zebin You, Xiaolu Zhang, Jingyang Ou, Jun Hu, Jun Zhou, Yankai Lin, Ji-Rong Wen, and Chongxuan Li. 2025. [Large language diffusion models](#). *Preprint*, arXiv:2502.09992.
- Matthew Niedoba, Berend Zwartsenberg, Kevin Patrick Murphy, and Frank Wood. 2025. [Towards a mechanistic explanation of diffusion model generalization](#). In *Forty-second International Conference on Machine Learning*.
- nostalgebraist. 2020. Interpreting gpt: the logit lens. *lesswrong*.
- Chris Olah, Nick Cammarata, Ludwig Schubert, Gabriel Goh, Michael Petrov, and Shan Carter. 2020. [Zoom in: An introduction to circuits](#). *Distill*. <https://distill.pub/2020/circuits/zoom-in>.
- OpenAI, Josh Achiam, Steven Adler, Sandhini Agarwal, Lama Ahmad, Ilge Akkaya, Florencia Leoni Aleman, Diogo Almeida, Janko Altschmidt, Sam Altman, Shyamal Anadkat, Red Avila, Igor Babuschkin,

- Suchir Balaji, Valerie Balcom, Paul Baltescu, Haiming Bao, Mohammad Bavarian, Jeff Belgum, Irwan Bello, Jake Berdine, Gabriel Bernadett-Shapiro, Christopher Berner, Lenny Bogdonoff, Oleg Boiko, Madelaine Boyd, Anna-Luisa Brakman, Greg Brockman, Tim Brooks, Miles Brundage, Kevin Button, Trevor Cai, Rosie Campbell, Andrew Cann, Brittany Carey, Chelsea Carlson, Rory Carmichael, Brooke Chan, Che Chang, Fotis Chantzis, Derek Chen, Sully Chen, Ruby Chen, Jason Chen, Mark Chen, Ben Chess, Chester Cho, Casey Chu, Hyung Won Chung, Dave Cummings, Jeremiah Currier, Yunxing Dai, Cory Decareaux, Thomas Degry, Noah Deutsch, Damien Deville, Arka Dhar, David Dohan, Steve Dowling, Sheila Dunning, Adrien Ecoffet, Atty Eleti, Tyna Eloundou, David Farhi, Liam Fedus, Niko Felix, Simón Posada Fishman, Juston Forte, Isabella Fulford, Leo Gao, Elie Georges, Christian Gibson, Vik Goel, Tarun Gogineni, Gabriel Goh, Rapha Gontijo-Lopes, Jonathan Gordon, Morgan Grafstein, Scott Gray, Ryan Greene, Joshua Gross, Shixiang Shane Gu, Yufei Guo, Chris Hallacy, Jesse Han, Jeff Harris, Yuchen He, Mike Heaton, Johannes Heidecke, Chris Hesse, Alan Hickey, Wade Hickey, Peter Hoeschele, Brandon Houghton, Kenny Hsu, Shengli Hu, Xin Hu, Joost Huizinga, Shantanu Jain, Shawn Jain, Joanne Jang, Angela Jiang, Roger Jiang, Haozhun Jin, Denny Jin, Shino Jomoto, Billie Jonn, Heewoo Jun, Tomer Kaftan, Łukasz Kaiser, Ali Kamali, Ingmar Kanitscheider, Nitish Shirish Keskar, Tabarak Khan, Logan Kilpatrick, Jong Wook Kim, Christina Kim, Yongjik Kim, Jan Hendrik Kirchner, Jamie Kiros, Matt Knight, Daniel Kokotajlo, Łukasz Kondraciuk, Andrew Kondrich, Aris Konstantinidis, Kyle Kosic, Gretchen Krueger, Vishal Kuo, Michael Lampe, Ikai Lan, Teddy Lee, Jan Leike, Jade Leung, Daniel Levy, Chak Ming Li, Rachel Lim, Molly Lin, Stephanie Lin, Mateusz Litwin, Theresa Lopez, Ryan Lowe, Patricia Lue, Anna Makanju, Kim Malfacini, Sam Manning, Todor Markov, Yaniv Markovski, Bianca Martin, Katie Mayer, Andrew Mayne, Bob McGrew, Scott Mayer McKinney, Christine McLeavey, Paul McMillan, Jake McNeil, David Medina, Aalok Mehta, Jacob Menick, Luke Metz, Andrey Mishchenko, Pamela Mishkin, Vinnie Monaco, Evan Morikawa, Daniel Mossing, Tong Mu, Mira Murati, Oleg Murk, David Mély, Ashvin Nair, Reiichiro Nakano, Rajeef Nayak, Arvind Neelakantan, Richard Ngo, Hyeonwoo Noh, Long Ouyang, Cullen O’Keefe, Jakub Pachocki, Alex Paino, Joe Palermo, Ashley Pantuliano, Giambattista Parascandolo, Joel Parish, Emy Parparita, Alex Passos, Mikhail Pavlov, Andrew Peng, Adam Perialman, Filipe de Avila Belbute Peres, Michael Petrov, Henrique Ponde de Oliveira Pinto, Michael, Pokorny, Michelle Pokrass, Vitchyr H. Pong, Tolly Powell, Alethea Power, Boris Power, Elizabeth Proehl, Raul Puri, Alec Radford, Jack Rae, Aditya Ramesh, Cameron Raymond, Francis Real, Kendra Rimbach, Carl Ross, Bob Rotsted, Henri Roussez, Nick Ryder, Mario Saltarelli, Ted Sanders, Shibani Santurkar, Girish Sastry, Heather Schmidt, David Schnurr, John Schulman, Daniel Selsam, Kyla Sheppard, Toki Sherbakov, Jessica Shieh, Sarah Shoker, Pranav Shyam, Szymon Sidor, Eric Sigler, Maddie Simens, Jordan Sitkin, Katarina Slama, Ian Sohl, Benjamin Sokolowsky, Yang Song, Natalie Staudacher, Felipe Petroski Such, Natalie Summers, Ilya Sutskever, Jie Tang, Nikolas Tezak, Madeleine B. Thompson, Phil Tillet, Amin Tootoonchian, Elizabeth Tseng, Preston Tuggle, Nick Turley, Jerry Tworek, Juan Felipe Cerón Uribe, Andrea Vallone, Arun Vijayvergiya, Chelsea Voss, Carroll Wainwright, Justin Jay Wang, Alvin Wang, Ben Wang, Jonathan Ward, Jason Wei, CJ Weinmann, Akila Welihinda, Peter Welinder, Jiayi Weng, Lilian Weng, Matt Wiethoff, Dave Willner, Clemens Winter, Samuel Wolrich, Hannah Wong, Lauren Workman, Sherwin Wu, Jeff Wu, Michael Wu, Kai Xiao, Tao Xu, Sarah Yoo, Kevin Yu, Qiming Yuan, Wojciech Zaremba, Rowan Zellers, Chong Zhang, Marvin Zhang, Shengjia Zhao, Tianhao Zheng, Juntang Zhuang, William Zhuk, and Barret Zoph. 2024. [Gpt-4 technical report](#). *Preprint*, arXiv:2303.08774.
- Yixin Ou, Yunzhi Yao, Ningyu Zhang, Hui Jin, Jiacheng Sun, Shumin Deng, Zhenguo Li, and Huajun Chen. 2025. [How do llms acquire new knowledge? a knowledge circuits perspective on continual pre-training](#). In *ACL (Findings)*, pages 19889–19913.
- Nikhil Prakash, Tamar Rott Shaham, Tal Haklay, Yonatan Belinkov, and David Bau. 2024. [Fine-tuning enhances existing mechanisms: A case study on entity tracking](#). *ArXiv*, abs/2402.14811.
- Qwen, :, An Yang, Baosong Yang, Beichen Zhang, Binyuan Hui, Bo Zheng, Bowen Yu, Chengyuan Li, Dayiheng Liu, Fei Huang, Haoran Wei, Huan Lin, Jian Yang, Jianhong Tu, Jianwei Zhang, Jianxin Yang, Jiayi Yang, Jingren Zhou, Junyang Lin, Kai Dang, Keming Lu, Keqin Bao, Kexin Yang, Le Yu, Mei Li, Mingfeng Xue, Pei Zhang, Qin Zhu, Rui Men, Runji Lin, Tianhao Li, Tianyi Tang, Tingyu Xia, Xingzhang Ren, Xuancheng Ren, Yang Fan, Yang Su, Yichang Zhang, Yu Wan, Yuqiong Liu, Zeyu Cui, Zhenru Zhang, and Zihan Qiu. 2025. [Qwen2.5 technical report](#). *Preprint*, arXiv:2412.15115.
- Alec Radford, Jeff Wu, Rewon Child, David Luan, Dario Amodei, and Ilya Sutskever. 2019. [Language models are unsupervised multitask learners](#).
- Marc’Aurelio Ranzato, Sumit Chopra, Michael Auli, and Wojciech Zaremba. 2016. [Sequence level training with recurrent neural networks](#).
- Subham Sekhar Sahoo, Marianne Arriola, Aaron Gokaslan, Edgar Mariano Marroquin, Alexander M Rush, Yair Schiff, Justin T Chiu, and Volodymyr Kuleshov. 2024. [Simple and effective masked diffusion language models](#). In *The Thirty-eighth Annual Conference on Neural Information Processing Systems*.
- Yingdong Shi, Changming Li, Yifan Wang, Yongxiang Zhao, Anqi Pang, Sibe Yang, Jingyi Yu, and Kan Ren. 2025. [Dissecting and Mitigating Diffusion Bias via Mechanistic Interpretability](#). In *2025 IEEE/CVF*

- Conference on Computer Vision and Pattern Recognition (CVPR)*, pages 8192–8202, Los Alamitos, CA, USA. IEEE Computer Society.
- Aaquib Syed, Can Rager, and Arthur Conmy. 2024. [Attribution patching outperforms automated circuit discovery](#). In *Proceedings of the 7th BlackboxNLP Workshop: Analyzing and Interpreting Neural Networks for NLP*, pages 407–416, Miami, Florida, US. Association for Computational Linguistics.
- Curt Tigges, Michael Hanna, Qinan Yu, and Stella Biderman. 2024. [LLM circuit analyses are consistent across training and scale](#). In *The Thirty-eighth Annual Conference on Neural Information Processing Systems*.
- Hugo Touvron, Louis Martin, Kevin Stone, Peter Albert, Amjad Almahairi, Yasmine Babaei, Nikolay Bashlykov, Soumya Batra, Prajjwal Bhargava, Shruti Bhosale, Dan Bikel, Lukas Blecher, Cristian Canton Ferrer, Moya Chen, Guillem Cucurull, David Esiobu, Jude Fernandes, Jeremy Fu, Wenyin Fu, Brian Fuller, Cynthia Gao, Vedanuj Goswami, Naman Goyal, Anthony Hartshorn, Saghar Hosseini, Rui Hou, Hakan Inan, Marcin Kardas, Viktor Kerkez, Madian Khabsa, Isabel Kloumann, Artem Korenev, Punit Singh Koura, Marie-Anne Lachaux, Thibaut Lavril, Jenya Lee, Diana Liskovich, Yinghai Lu, Yuning Mao, Xavier Martinet, Todor Mihaylov, Pushkar Mishra, Igor Molybog, Yixin Nie, Andrew Poulton, Jeremy Reizenstein, Rashi Rungta, Kalyan Saladi, Alan Schelten, Ruan Silva, Eric Michael Smith, Ranjan Subramanian, Xiaoqing Ellen Tan, Binh Tang, Ross Taylor, Adina Williams, Jian Xiang Kuan, Puxin Xu, Zheng Yan, Iliyan Zarov, Yuchen Zhang, Angela Fan, Melanie Kambadur, Sharan Narang, Aurelien Rodriguez, Robert Stojnic, Sergey Edunov, and Thomas Scialom. 2023. [Llama 2: Open foundation and fine-tuned chat models](#). *Preprint*, arXiv:2307.09288.
- Ashish Vaswani, Noam Shazeer, Niki Parmar, Jakob Uszkoreit, Llion Jones, Aidan N Gomez, Łukasz Kaiser, and Illia Polosukhin. 2017. [Attention is all you need](#). In *Advances in Neural Information Processing Systems*, volume 30. Curran Associates, Inc.
- Kevin Ro Wang, Alexandre Variengien, Arthur Conmy, Buck Shlegeris, and Jacob Steinhardt. 2023. [Interpretability in the wild: a circuit for indirect object identification in GPT-2 small](#). In *The Eleventh International Conference on Learning Representations*.
- Xu Wang, Yan Hu, Wenyu Du, Reynold Cheng, Benyou Wang, and Difan Zou. 2025. [Towards understanding fine-tuning mechanisms of llms via circuit analysis](#). *ArXiv*, abs/2502.11812.
- Sean Welleck, Ilya Kulikov, Stephen Roller, Emily Dinan, Kyunghyun Cho, and Jason Weston. 2019. [Neural text generation with unlikelihood training](#).
- Jiacheng Ye, Jiahui Gao, Shansan Gong, Lin Zheng, Xin Jiang, Zhenguo Li, and Lingpeng Kong. 2025a. [Beyond autoregression: Discrete diffusion for complex reasoning and planning](#). In *The Thirteenth International Conference on Learning Representations*.
- Jiacheng Ye, Zhihui Xie, Lin Zheng, Jiahui Gao, Zirui Wu, Xin Jiang, Zhenguo Li, and Lingpeng Kong. 2025b. [Dream 7b: Diffusion large language models](#). *Preprint*, arXiv:2508.15487.

A Dataset Details

Datasets For the *countdown* task, we evaluate both LLaMA-series and Qwen-series models using 500 evaluation examples per model. For LLaMA-series models, we use 13 diffusion steps, which correspond to 13 tokens (diffusion step = token). For Qwen-series models, we use 12 diffusion steps, corresponding to 12 tokens. For the *IOI* task, we evaluate 500 examples in a single-step setting with 1 diffusion step and 1 token.

B Experimental Details and Results

Computational Resources All experiments were conducted on NVIDIA A6000 GPUs. Circuit extraction and analysis required less than 10 GPU-hours per model. No additional pre-training was performed.

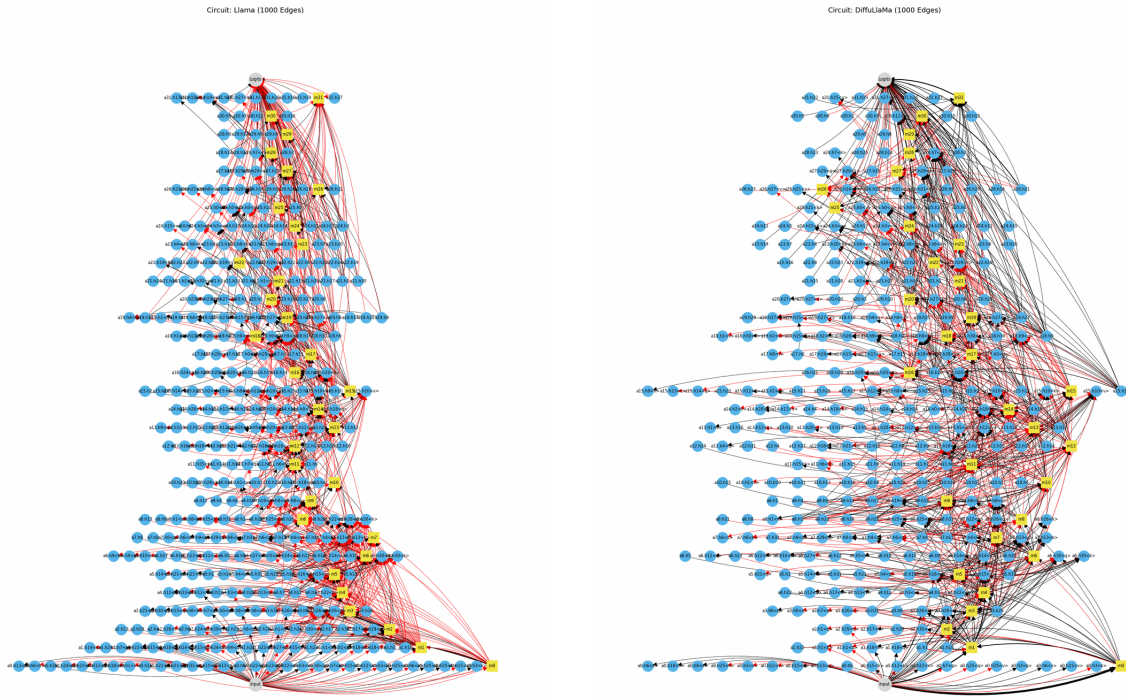
Implementation Details Our experiments use HuggingFace Transformers for model loading and inference. Circuit discovery is implemented using Edge Attribution Patching with Integrated Gradients (EAP-IG), where we select the top 1,000 edges (corresponding to a faithfulness score of 0.6) ranked by attribution scores as a trade-off between sparsity and attribution coverage. Empirically, smaller thresholds lead to unstable circuit structures, while larger thresholds rapidly approach the full graph without improving interpretability. The choice of 1,000 edges lies in a stable regime where circuit topology and component rankings remain consistent.

Attribution scores are then aggregated at the component level to identify the Top-K components. We set $K = 100$, corresponding to the smallest value for which the selected components form a well-connected circuit, ensuring that the resulting subgraph remains interpretable while preserving end-to-end connectivity. Logit lens projections follow the standard unembedding-based formulation. All other parameters follow default settings from the respective libraries.

Licenses and Terms of Use All pretrained models and tools used in this work are publicly released research artifacts. We use them solely for research and analysis purposes, in accordance with their respective licenses, and do not redistribute any models or derived data.

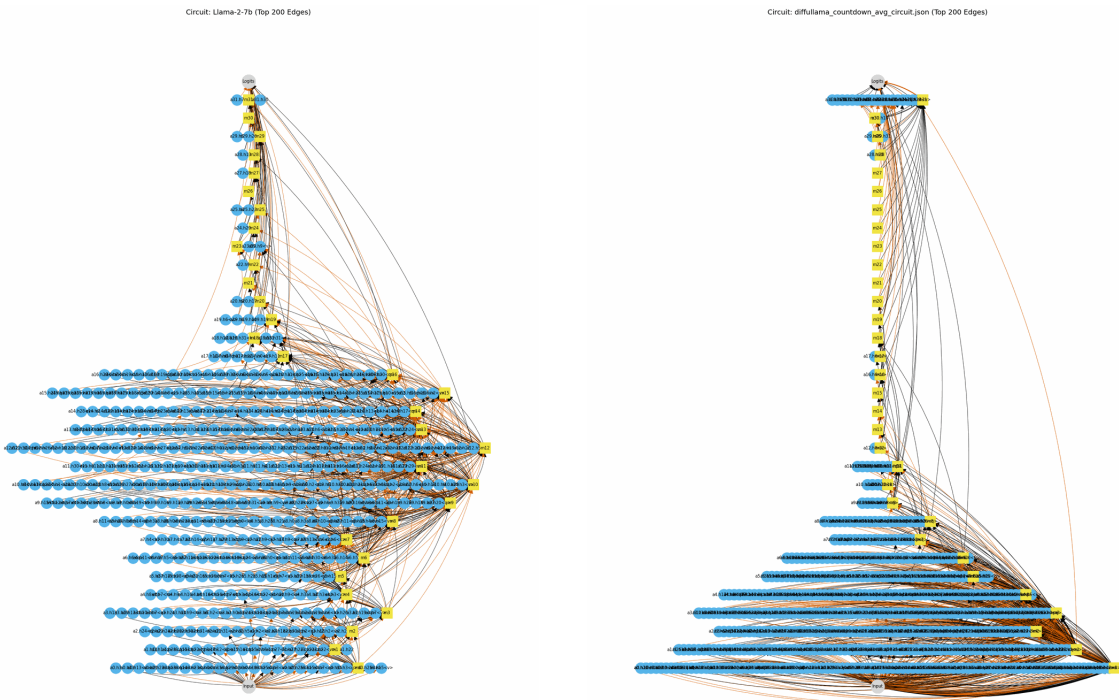
Step-wise Circuit Stability For analyses involving step-wise circuit extraction, we compute cir-

cuits at each diffusion step and then aggregate attribution scores across steps. We find that the set of participating components (attention heads and MLP layers) remains largely stable over diffusion time, with more than 90% overlap in selected components between steps. Accordingly, the step-wise circuit visualizations shown in Figures 6 and 5 represent averaged structures, while step-wise variation is primarily reflected in changes to the attributed edges rather than in the identity of the components themselves. This suggests that masked diffusion primarily refines information routing among a largely fixed component set, rather than progressively recruiting new components.



(a) IOI — Llama-2-7B

(b) IOI — DiffuLlama-7B



(c) Countdown — LLaMA-2-7B

(d) Countdown — DiffuLLaMA-7B

Figure 4: Circuit comparison across tasks and architectures. Top: IOI. Bottom: COUNTDOWN. Left: Autoregressive (LLaMA-2-7B). Right: Masked Diffusion (DiffuLLaMA).

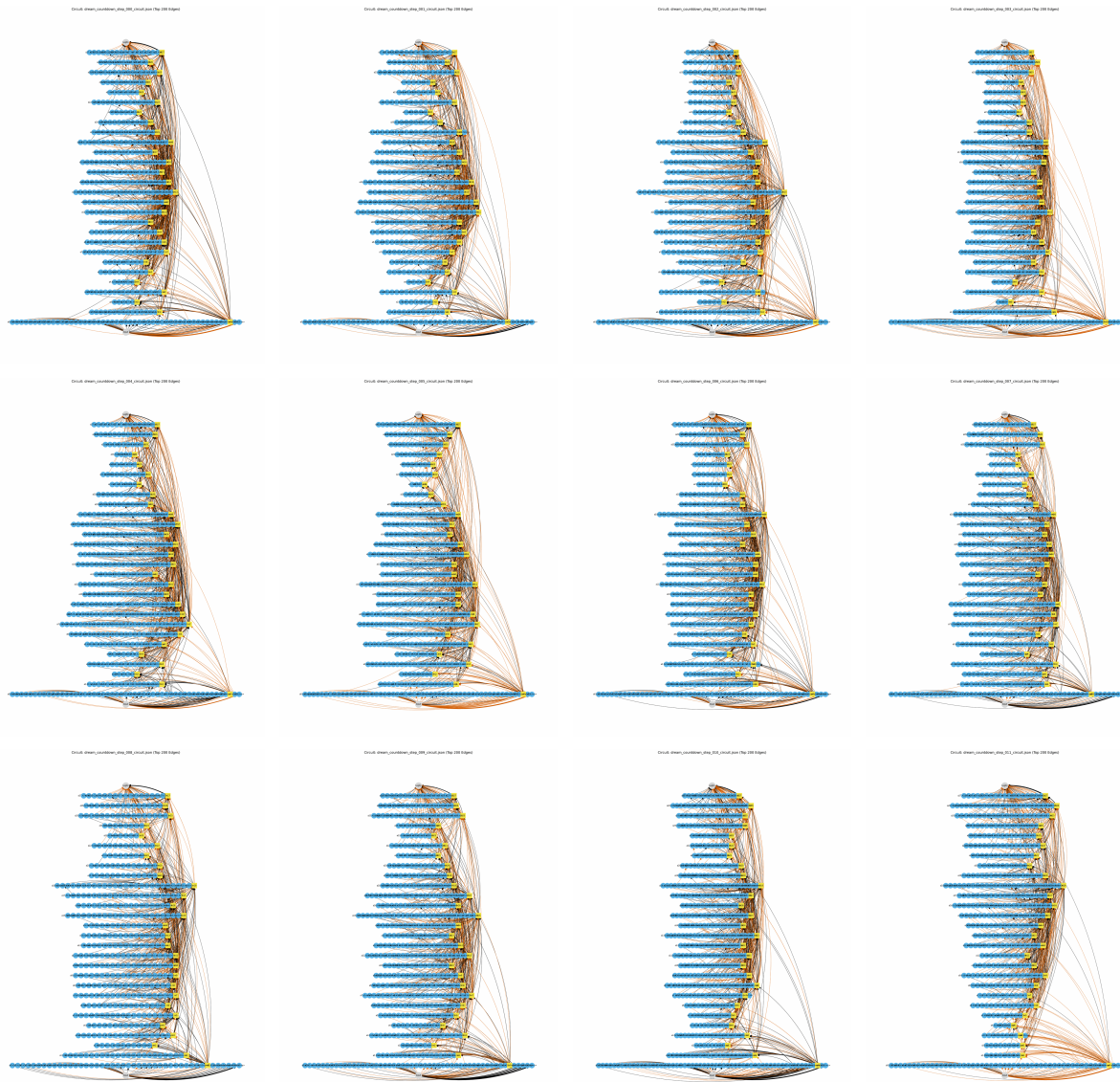


Figure 5: step-wise circuit visualization of Dream on the COUNTDOWN task. Steps 1–12 are shown from left to right and top to bottom.

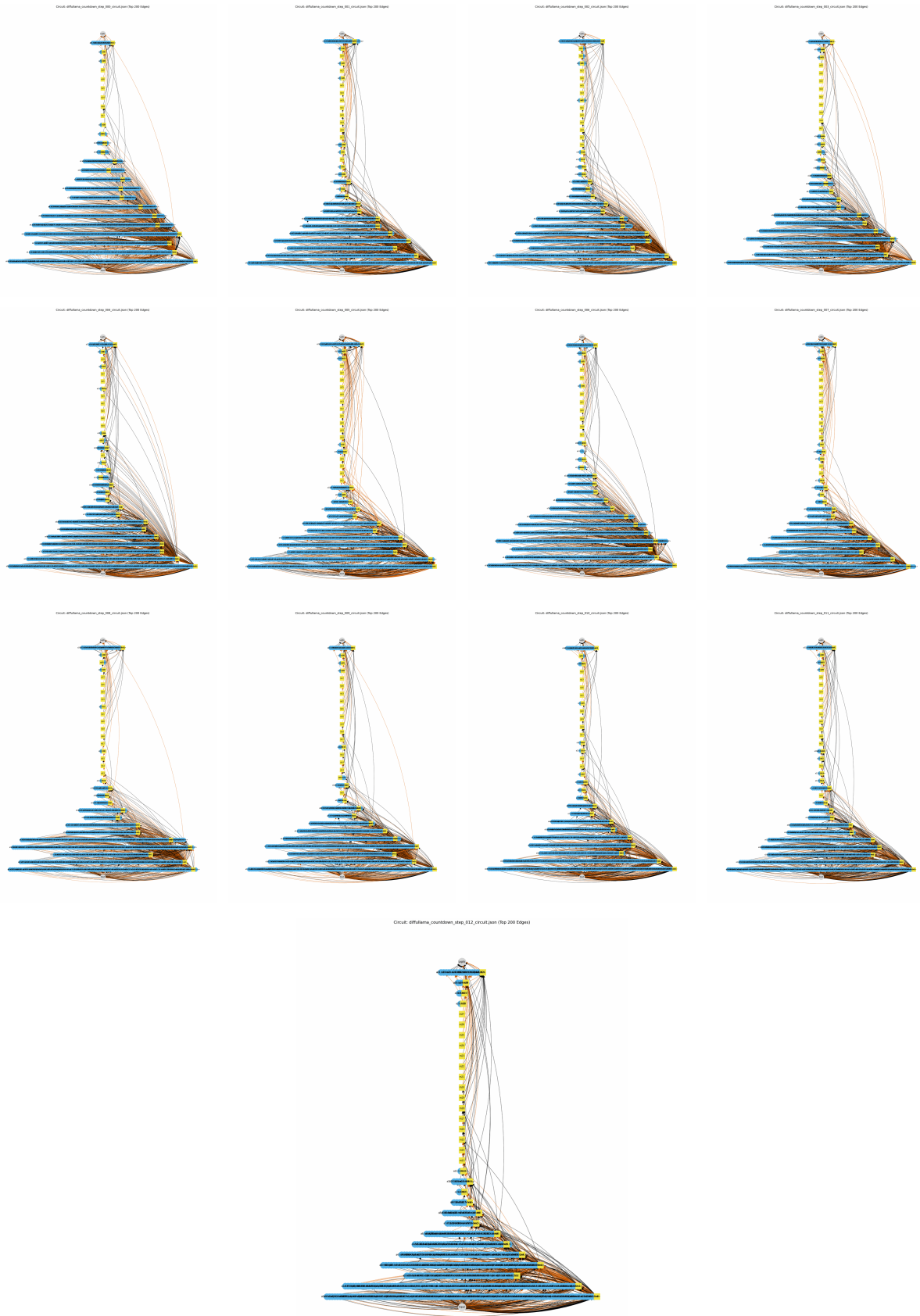


Figure 6: step-wise circuit visualization of DiffuLLaMA on the COUNTDOWN task. Steps 1–12 are shown from left to right and top to bottom.

Table 3: Top 30 Source Components for IOI Task

Model	Top Source Components (Edges)
LLaMA-2	input→m0, input→m1, a3.h26→m3, a26.h21→logits, m1→a3.h26< q >, a1.h18→m1, input→a3.h26< q >, a25.h0→logits, m27→logits, a27.h29→logits, m0→m1, m1→a3.h26< k >, a5.h15→a6.h30< k >, input→a3.h26< k >, a24.h3→logits, a23.h20→logits, a21.h30→logits, a1.h1→m1, m2→a3.h26< k >, m0→a3.h26< q >, a18.h9→logits, a21.h1→logits, m2→a3.h26< q >, m4→a6.h30< q >, m0→a3.h26< k >, m0→a1.h18< q >, input→a1.h18< q >, a1.h1→a3.h26< q >, a24.h15→logits, a20.h8→logits
Qwen	a24.h24→logits, a26.h15→logits, a23.h11→logits, a27.h21→logits, a27.h4→logits, m27→logits, a27.h1→logits, a26.h26→logits, a26.h22→logits, m20→m22, a27.h18→logits, a27.h17→logits, a27.h5→logits, a27.h14→logits, a24.h23→logits, m24→logits, input→a0.h10< v >, a27.h3→logits, a20.h24→m22, a27.h24→logits, a17.h24→a20.h24< v >, a26.h5→logits, input→a0.h3< v >, a27.h4→m27, m25→logits, a25.h24→logits, a18.h25→a20.h24< v >, a18.h27→a20.h24< v >, a26.h2→logits, m22→a25.h25< q >
DiffuLLaMA	input→m0, input→m1, a3.h26→m3, a28.h7→logits, m31→logits, a26.h21→logits, m0→m1, a1.h18→m1, a27.h29→logits, m1→a3.h26< q >, a1.h1→m1, a5.h15→a6.h30< k >, m1→a3.h26< k >, m1→m4, input→a3.h26< q >, input→a3.h26< k >, a26.h14→logits, m2→a3.h26< k >, a30.h12→logits, m4→a6.h30< q >, m0→a3.h26< q >, a23.h20→logits, a18.h9→a28.h7< v >, input→a1.h18< q >, m0→a1.h18< q >, input→m4, m2→a3.h26< q >, a22.h19→logits, input→m2, a27.h29→a28.h7< v >
Dream	a24.h24→logits, m19→m20, a23.h10→logits, m18→m19, m19→m21, m9→m19, m21→m22, a18.h25→m20, m14→m15, m25→logits, m12→m18, m7→m17, a15.h20→m16, m9→m20, m10→m20, a15.h20→m20, m12→m15, m12→m13, m18→m22, m17→m20, m14→m22, a15.h20→m19, a15.h23→m16, m8→m17, m11→m16, m21→logits, a25.h24→logits, a18.h25→m21, m8→m20, m11→m20

Table 4: Top 30 Source Components for COUNTDOWN Task

Model	Top Source Components (Edges)
LLaMA-2	input→a0.h15< v >, m10→m11, m11→m12, a1.h22→m1, m6→m11, m11→m15, input→a0.h25< v >, m0→a1.h22< v >, m29→logits, m7→m9, m0→m2, m28→logits, m8→m12, m8→a11.h29< v >, m8→m11, a2.h2→m3, m3→m5, m14→m15, m0→m1, input→a0.h3< q >, m13→m15, a12.h5→m13, m7→m10, a12.h22→m12, a5.h15→a7.h6< k >, input→a2.h2< v >, m24→logits, m0→a1.h22< k >, m12→m14, m7→a8.h15< v >
Qwen	m26→logits, m25→logits, m27→logits, input→a0.h3< v >, a23.h11→logits, a25.h12→logits, a26.h22→logits, m24→logits, a26.h24→logits, m26→m27, a24.h23→logits, m21→a23.h11< v >, a0.h3→m0, a22.h13→logits, a26.h23→logits, a23.h11→m25, m25→m27, a23.h19→logits, a25.h12→m27, a26.h25→logits, m21→a25.h12< v >, m20→a23.h11< v >, a26.h26→logits, m25→a26.h22< v >, a23.h11→m26, a26.h22→m27, a26.h22→m26, a26.h24→m27, a23.h11→a26.h22< v >, a24.h23→m25
DiffuLLaMA	m1→m2, input→m0, m1→m3, input→a0.h12< k >, m31→logits, m1→a4.h5< k >, input→a0.h3< k >, input→a0.h15< v >, m1→a3.h3< q >, m1→a3.h27< q >, input→m1, input→a0.h0< k >, input→a0.h3< q >, input→a0.h1< v >, input→a1.h1< v >, m1→a3.h26< k >, m1→a3.h7< k >, m1→a3.h8< k >, m1→m4, m0→m1, m1→a4.h5< q >, input→a0.h13< q >, m1→a2.h2< k >, m0→m3, m1→a3.h0< q >, input→a0.h3< v >, m1→a6.h20< k >, input→a0.h13< v >, m1→a3.h17< k >, m1→a5.h23< q >
Dream	m25→logits, m27→logits, m26→logits, input→a0.h15< q >, a0.h10→m0, input→a0.h3< v >, m24→logits, input→a0.h10< v >, m23→logits, input→a0.h11< q >, input→a0.h15< k >, input→a0.h15< v >, a0.h3→m0, a25.h12→logits, m0→m1, m26→m27, input→a0.h0< v >, input→a0.h11< v >, a27.h11→logits, a26.h22→logits, a26.h25→logits, m22→logits, m21→m27, a0.h15→m0, input→a0.h11< k >, m25→m26, m22→m27, a25.h12→m27, input→a0.h10< k >, a26.h24→logits

Table 5: Top interpretable tokens for high-attribution components (excluding components stated in table 2). Components are sorted by confidence (probability of the top token).

Task	Model	Comp.	Top Tokens (Probability)	
Countdown	DiffuLLaMA	m1	sierp (0.936), kwiet (0.045), Hinweis (0.004)	
		m2	(U+207B) (5.6e-05), nahm (5.6e-05), Hinweis (5.5e-05)	
		m3	iftung (4.1e-05), (U+043D) (U+0434) (U+0434) (4.1e-05), iation (4.1e-05)	
		input	rd (3.7e-05), iation (3.7e-05), ness (3.7e-05)	
		m0	mes (3.5e-05), led (3.5e-05), med (3.5e-05)	
		Dream	m25	out (0.012),)) (0.001), from (0.001)
			m26	, - (7.9e-04), A (7.3e-04), S (6.3e-04)
			m22	nothing (8.7e-05), H (8.6e-05), a (7.2e-05)
			m24	int (8.3e-05), i (7.3e-05), commemor (6.5e-05)
			m21	= (3.2e-05), by (3.1e-05), C (3.0e-05)
	a27.h11		doen (2.9e-05), uteur (2.6e-05), retali (2.4e-05)	
	a25.h12		7 (2.2e-05), 8 (1.9e-05), 3 (1.7e-05)	
	a26.h22		cosy (2.0e-05), W (1.9e-05), -ok (1.8e-05)	
	a26.h25		fourth (1.4e-05), five (1.4e-05), IV (1.4e-05)	
	a26.h24		ist (1.2e-05), /S (1.2e-05), SIX (1.2e-05)	
	LLaMA-2	m1	sierp (0.896), Unterscheidung (0.074), kwiet (0.027)	
		m24	them (0.009), ihnen (0.004), they (0.003)	
		m28	- (0.006), , (0.005), - (0.004)	
		m14	/- (7.7e-04), +- (2.2e-04), ÿ (2.0e-04)	
		m15	by (2.7e-04), look (2.1e-04), > (1.5e-04)	
m13		Halle (1.7e-04), Hook (1.2e-04), wa (1.1e-04)		
m11		attan (1.4e-04), iore (1.1e-04), (U+0442) (U+043A) (U+0443) (1.0e-04)		
m12		ieder (1.1e-04), ikai (1.1e-04), sail (1.1e-04)		
m7		bek (9.7e-05), untime (7.7e-05), mina (7.5e-05)		
m9		opsis (8.7e-05), P0 (8.2e-05), zug (7.7e-05)		
m10	ador (8.4e-05), rok (8.3e-05), keit (8.3e-05)			
m8	concrete (8.3e-05), OST (8.1e-05), Chor (8.0e-05)			
m6	idenote (7.2e-05), ischof (7.1e-05), asm (7.1e-05)			
m0	bolds (6.6e-05), sce (6.0e-05), hina (5.7e-05)			
m5	kop (6.6e-05), ō (6.3e-05), Sug (6.2e-05)			
m2	nobody (6.5e-05), nahm (6.0e-05), everybody (6.0e-05)			
m3	uche (5.2e-05), Chronology (5.1e-05), emer (4.9e-05)			
a12.h5	extension (3.9e-05), oba (3.9e-05), extensions (3.9e-05)			
a5.h15	Campbell (3.8e-05), beskre (3.7e-05), : (U+2009) (3.7e-05)			
input	/- (3.7e-05), igny (3.6e-05), Extern (3.6e-05)			
a1.h22	(U+045A)y (3.4e-05), (U+4E0B) (3.4e-05), unci (3.4e-05)			

Continued on next page

Table 5 – continued from previous page

Task	Model	Comp.	Top Tokens (Probability)	
	Qwen	a12.h22	tel (3.4e-05), (3.3e-05), guez (3.3e-05)	
		a2.h2	zik (3.2e-05), Muse (3.2e-05), èn (3.2e-05)	
		m26	(U+6027)(U+4EF7) (1.000), B (1.000), & (0.999)	
		m27	Human (1.000), ^K (1.000), derive (0.999)	
		m24	(U+62EC) (0.973), (U+5973)(U+6027)(U+670B)(U+53CB) (0.955), .ImageAlign (0.914)	
		m21	aeda (0.608), so (0.599), to (0.306)	
		a26.h24	A (0.032), A (0.006), (G (0.004)	
		a26.h23	make (0.008), (make (0.008), .make (0.006)	
		a26.h26	-await (4.0e-04), XMLElement (3.2e-04), etail (2.7e-04)	
		m0	fkk (3.5e-04), libertine (2.8e-04), [];\n (2.3e-04)	
		a26.h25	(U+81EA)(U+52A8)(U+751F)(U+6210) (3.1e-04), /Dk (2.5e-04), line (2.4e-04)	
		a26.h22	(U+5341)(U+56DB) (1.9e-04), (U+5341)(U+4E09) (1.8e-04), (U+80B2)(U+4EBA) (1.6e-04)	
		a25.h12	4 (1.5e-04), 5 (1.4e-04), Fifth (1.2e-04)	
		a23.h19	Five (7.1e-05), five (5.0e-05), 5 (4.1e-05)	
		a24.h23	num (2.5e-05), Gall (2.5e-05), num (2.4e-05)	
		a0.h3	teenth (2.4e-05), bénéficié (1.9e-05), Noticed (1.9e-05)	
		a23.h11	...";\n (1.3e-05), #ac (1.2e-05), aź (1.2e-05)	
		input	(U+304D)(U+3061)(U+3093) (9.0e-06), (U+4E26)(U+4E14) (9.0e-06), (U+6362)(U+53E5)(U+8BDD) (9.0e-06)	
IOI		DiffuLLaMA	m1	sierp (0.550), kwiet (0.155), Hinweis (0.032)
			m31	in (0.204), to (0.044), \n (0.039)
	a23.h20		Sarah (3.8e-04), Vir (1.1e-04), sar (1.1e-04)	
	a28.h7		V (2.9e-04), K (2.0e-04), Kim (2.0e-04)	
	a26.h14		David (1.7e-04), David (1.4e-04), dav (1.2e-04)	
	a30.h12		William (1.3e-04), Will (1.2e-04), Will (1.1e-04)	
	m4		disambiguation (1.1e-04), printStackTrace (9.8e-05), - (9.5e-05)	
	m2		nahm (5.5e-05), - (5.5e-05), Hinweis (5.4e-05)	
	a27.h29		urn (5.4e-05), urr (5.3e-05), enis (4.9e-05)	
	a18.h9		owo (5.1e-05), ceu (4.3e-05), fen (4.3e-05)	
	m3		(U+4F1D) (3.5e-05), tu (3.5e-05), adr (3.5e-05)	
	a5.h15		temps (3.4e-05), vend (3.4e-05), cancel (3.4e-05)	
	a3.h26		lex (3.3e-05), ongodb (3.3e-05), huvudstaden (3.3e-05)	
	input		ô (3.3e-05), Horn (3.3e-05), roid (3.3e-05)	
	m0		Einzeln (3.3e-05), (U+800C) (3.3e-05), atri (3.3e-05)	
	a1.h1		(U+4EA4) (3.2e-05), gate (3.2e-05), Moc (3.2e-05)	
	a1.h18		(3.2e-05), jsp (3.2e-05), epen (3.2e-05)	
	Dream		m21	pliers (1.4e-05), Tap (1.4e-05), ynom (1.3e-05)
	m13	doen (1.1e-05), bourgeois (1.1e-05), upholstery (1.0e-05)		
	m8	wooded (1.1e-05), curt (1.0e-05), Genius (1.0e-05)		

Continued on next page

Table 5 – continued from previous page

Task	Model	Comp.	Top Tokens (Probability)
		m9	melodies (1.1e-05), interpolate (1.0e-05), Infantry (1.0e-05)
		m10	forestry (1.0e-05), rhet (1.0e-05), doen (1.0e-05)
		m15	orestation (1.0e-05), secluded (9.0e-06), cosy (9.0e-06)
		m18	Races (1.0e-05), weets (9.0e-06), ife (9.0e-06)
		m19	adjud (1.0e-05), enchanted (1.0e-05), instantiate (1.0e-05)
		m20	blot (1.0e-05), oval (1.0e-05), blinking (1.0e-05)
		m7	glimps (1.0e-05), seeding (1.0e-05), sadd (1.0e-05)
		m11	Tweet (9.0e-06), Intr (9.0e-06), enchanted (8.0e-06)
		m12	milit (9.0e-06), bourgeois (9.0e-06), slashes (9.0e-06)
		m14	enam (9.0e-06), upholstery (9.0e-06), vener (9.0e-06)
		m16	lan (9.0e-06), part (9.0e-06), ocal (9.0e-06)
		m17	Israelis (9.0e-06), commemor (9.0e-06), driv (9.0e-06)
		a23.h10	(8.0e-06), - (8.0e-06), ø (8.0e-06)
		a24.h24	i (8.0e-06), in (8.0e-06), on (8.0e-06)
		a15.h20	's (7.0e-06), home (7.0e-06), half (7.0e-06)
		a15.h23	doen (7.0e-06), Packages (7.0e-06), classy (7.0e-06)
		a18.h25	ropy (7.0e-06), liner (7.0e-06), Bio (7.0e-06)
		a25.h24	mailed (7.0e-06), RSS (7.0e-06), masturbating (7.0e-06)
	LLaMA-2	m1	sierp (0.865), Unterscheidung (0.110), kwiet (0.022)
		m27	too (0.394), her (0.042), e (0.031)
		a26.h21	Marian (0.076), Pat (0.008), Anne (0.008)
		a25.h0	Richard (0.050), William (0.035), David (0.033)
		a24.h3	Rosa (0.007), Williams (6.4e-04), Alice (6.1e-04)
		a20.h8	Susan (0.004), sus (4.6e-04), suspect (1.4e-04)
		a23.h20	Sarah (0.004), Vir (0.001), vir (0.001)
		a21.h30	Lee (6.1e-04), Kelly (3.3e-04), ee (1.5e-04)
		m4	vy (2.1e-04), disambiguation (2.1e-04), - (2.0e-04)
		a27.h29	arta (1.3e-04), ML (1.3e-04), ignon (1.3e-04)
		a18.h9	Blue (9.5e-05), cyk (9.2e-05), nja (8.8e-05)
		m0	bolds (6.4e-05), sce (6.0e-05), partiellement (5.6e-05)
		m2	nobody (6.4e-05), nahm (5.9e-05), everybody (5.9e-05)
		m3	ime (5.4e-05), (U+82B1) (5.2e-05), ña (5.1e-05)
		input	ny (4.0e-05), ten (4.0e-05), eral (3.9e-05)
		a5.h15	Chronology (3.7e-05), :// (3.6e-05), Extern (3.6e-05)
		a3.h26	erea (3.6e-05), zət (3.6e-05), Songs (3.6e-05)
		a1.h1	(U+4EA4) (3.4e-05), Indep (3.3e-05), gate (3.3e-05)
		a1.h18	Bek (3.3e-05), arguments (3.3e-05), Millionen (3.3e-05)
	Qwen	m27	Human (1.000), Rossi (0.990), “ (0.978)
		m25	Alexander (1.000), shall (0.986), zá (0.970)
		m24	court (0.983), (U+5973) (U+6027) (U+670B) (U+53CB) (0.955), }) ; \n (0.941)

Continued on next page

Table 5 – continued from previous page

Task	Model	Comp.	Top Tokens (Probability)
		m22	thought (0.958), during (0.921), term (0.914)
		m20	(U+6027)(U+4EF7) (0.893), ", __ (0.247), ynos (0.101)
		a27.h17	Christina (0.444), Jessica (0.339), Crystal (0.330)
		a27.h18	Lisa (0.418), Elizabeth (0.282), Nic (0.228)
		a27.h1	Jamie (0.400), Nathan (0.345), Mary (0.275)
		a27.h21	Amy (0.360), Amber (0.331), Adam (0.331)
		a26.h5	Jesse (0.344), Nich (0.217), Rebecca (0.203)
		a27.h3	Katie (0.305), Ken (0.295), Brittany (0.189)
		a27.h14	Heather (0.252), Steven (0.244), Sean (0.223)
		a27.h24	Scott (0.233), Brad (0.221), Kris (0.220)
		a26.h2	Brad (0.227), Megan (0.194), brand (0.180)
		a27.h4	Mary (0.224), Ben (0.223), Mark (0.212)
		a26.h15	Danielle (0.215), Alicia (0.182), Dustin (0.176)
		a24.h23	John (0.013), Thomas (0.013), Kenneth (0.008)
		a25.h24	ch (0.002), William (0.001), w (0.001)
		a24.h24	Gad (0.001), ogen (9.4e-04), Aqu (8.7e-04)
		a26.h22	.AppSettings (6.5e-04), azt (6.0e-04), .d (4.3e-04)
		a26.h26	(U+0625)(U+0639)(U+062F)(U+0627)(U+062F) (1.9e-04), .TRAILING (1.8e-04), inx (1.8e-04)
		a18.h25	_locator (8.1e-05), ="' . (8.1e-05), .instrument (7.8e-05)
		a20.h24	setChecked (7.5e-05), anmar (6.5e-05), CAF (6.4e-05)
		a18.h27	(U+0623)(U+063A)(U+0644)(U+0628) (4.6e-05), dealloc (4.5e-05), (U+FFFD)(U+FFFD) (4.4e-05)
		a17.h24	.setCharacter (3.0e-05), -urlencoded (2.8e-05), entious (2.7e-05)
		input	(U+304D)(U+3061)(U+3093) (9.0e-06), (U+6362)(U+53E5)(U+8BDD) (9.0e-06), (U+4E26)(U+4E14) (9.0e-06)